Large Eddy Simulation of FDA's Idealized Medical Device

Yann T. Delorme, Kameswararao Anupindi, and Steven H. Frankel

School of Mechanical Engineering, Purdue University, West Lafayette, IN 47907, USA

Associate Editor Ajit P. Yoganathan oversaw the review of this article.

Abstract—A hybrid large eddy simulation and immersed boundary method (IBM) computational approach is used to make quantitative predictions of flow field statistics within the Food and Drug Administration's idealized medical device. An in-house code is used, hereafter (*WenoHemo*[TM]), that combines high-order finite-difference schemes on structured staggered Cartesian grids with an IBM to facilitate flow over or through complex stationary or rotating geometries and employs a subgrid-scale turbulence model that more naturally handles transitional flows (Delorme *et al.*, J Biomech 46:207–436, [2013]). Predictions of velocity and wall shear stress statistics are compared with previously published experimental measurements from Hariharan *et al.* (J Biomech Eng 133:041002, [2011]) for the four Reynolds numbers considered.

Keywords—Large eddy simulation, Idealized medical device, Turbulence, Shear stress, Transitional flow.

INTRODUCTION

The use of computational fluid dynamics (CFD) to study pathological and medical device hemodynamics has become widespread in the biomedical research community. This is in part due to the ability of CFD to predict flow patterns, wall shear stress, and particle residence times where experiments are not possible. The efficacy of CFD depends critically on its quantitative accuracy regarding not only global performance measures like pressure drop across a stenosis or pressure rise across a rotary blood pump but also regarding instantaneous flow features and velocity statistics. This is especially important regarding blood damage prediction particularly in the presence of a medical device. Accuracy of the numerical predictions is of primary importance, especially when trying to evaluate the performance of such a device.

The majority of CFD studies of pathological and medical device hemodynamics have employed Reynolds averaged Navier–Stokes (RANS) approach. This is most likely due to its computational affordability and availability in most commercial and open-source CFD codes, allowing patient-specific geometries and multi-physics, including blood damage modeling, to be addressed.[4] As a result of the fact that pathological and medical device hemodynamics typically involves complex, irregular flows featuring streamline curvature and rotation, as well as possible transition to turbulence, RANS models in many engineering application areas have historically had difficulties accurately predicting such flows features.[3] This was most recently evidenced in the inter-laboratory study related to measurements and modeling of flow fields associated with the Food and Drug Administration's (FDAs) idealized medical device.[12] In that study, CFD predictions either assumed laminar flow or used a RANS based turbulence models to directly predict the mean flow field and highlighted the need for better models of transition and the use of large eddy simulation (LES) to improve quantitative accuracy as summarized below.

In 2011, Hariharan *et al.*[6] studied the uncertainties related to experimental measurements in an idealized medical device. The goal of this FDA commissioned study was to compare experimental measurements between different laboratories in order to reference the key parameters that can influence experimental measurements. The nozzle model had characteristics of medical devices with blood flowing through them, such as hemodialysis tubing sets, catheters, cannulae, and hypodermic needles. The study was performed at different throat Reynolds number (Re_t) (500, 2000, 3500, 5000, and 6500) to cover a range

---

Address correspondence to Yann T. Delorme, School of Mechanical Engineering, Purdue University, West Lafayette, IN 47907, USA. Electronic mail: delorme.yann@gmail.com

of flows from laminar to turbulent. The study showed large differences between laboratories, especially in the laminar and transitional regions.

In 2012, Stewart et al.[12] presented results from a related studies between laboratories to assess current state of the art in CFD simulations applied to medical devices. RANS-based solvers were used with different turbulence models, and the results were compared to the experimental measurements from Hariharan et al.[6] For the laminar case, simulations were able to capture the absence of break down of the jet downstream of the sudden expansion. In the convergent section, all models performed well. At $Re_t = 2000$, only the k–ω turbulence model was able to accurately capture the location of the jet breakdown. All other turbulence models predicted premature breakdown. Proximal to the convergent section, only the laminar simulations were able to predict laminar velocity profiles as measured in the experiments. In the distal region of the throat, before the breakdown of the jet, only the laminar cases showed good agreement with the experiments. On the other hand, only the turbulent cases showed good agreement in the post-breakdown region. At the higher Re_t when the flow became fully turbulent, the different turbulence models performed better but the k–ω model underestimated the location of the breakdown of the jet. Most turbulence models were able to predict accurately the wall pressure, except for the laminar case, but accurate predictions of fluid and wall shear stresses were shown to be difficult. Most of the models showed peaks in magnitude up to 5 times larger than the experimental measurements.

In the present study, the LES approach is applied to the very same FDA idealized medical device and quantitative comparisons to the experimental data from Hariharan et al.[6] are made. An in-house code that features high-order numerical methods and an appropriate subgrid-scale (SGS) turbulence model capable of making predictions for transitional flows is employed. Four different Re_t cases (500, 2000, 3500, and 5000) are considered in what follows.

METHODS

Governing Equations

In LES the unsteady three-dimensional large-scale flow features are numerically resolved through appropriate grid and numerical method choices, whereas the effect of the unresolved small-scale flow features on the large-scale flow field are modeled using a SGS model. Hence, the governing equations to be solved in this study are the non-dimensional, filtered incompressible Navier–Stokes equations:

$$\frac{\partial \bar{u}_i}{\partial t} + \bar{u}_j \frac{\partial \bar{u}_i}{\partial x_j} = -\frac{\partial \bar{p}}{\partial x_i} + \frac{1}{Re}\frac{\partial \bar{u}_i}{\partial x_j \partial x_j} - \frac{\partial \tau_{ij}}{\partial x_j} \qquad (1)$$

$$\frac{\partial \bar{u}_i}{\partial x_i} = 0 \qquad (2)$$

where $\bar{u}_i$ and $\bar{p}$ are the filtered velocity and pressure, respectively, x_i ($i = 1, 2,$ or 3) are the Cartesian coordinates, Re is the Reynolds number, and τ_{ij} is the SGS stress tensor that arises from the filtering of the non-linear convection term and requires closure. The SGS stress tensor is defined as:

$$\tau_{ij} = \overline{u_i u_j} - \bar{u}_i \bar{u}_j - \frac{2}{6}(\overline{u_k u_k} - \bar{u}_k \bar{u}_k)\delta_{ij} \qquad (3)$$

and is modeled in this study as:

$$\tau_{ij} = -2v_T S_{ij} \qquad (4)$$

where v_T is the SGS eddy viscosity and S_{ij} is the filtered strain rate tensor. In the present study, the eddy viscosity is modeled using the constant coefficient Vreman model,[15] which was utilized and validated by Shetty et al.[10] for fully in-homogeneous turbulent flows. Details can be found in the cited references.

Numerical Approach

The closed filtered governing equations are numerically integrated using a fractional time stepping approach featuring a third-order accurate backward difference formula (BDF) scheme[11] for time advancement. Spatial discretization is achieved using a fifth-order accurate weighted-average non-oscillatory (WENO) finite-difference scheme[17] for convection and a fourth-order centered finite-difference scheme for diffusion. The pressure Poisson equation is solved using the MUDPACK[1] solver. The use of high-order finite-difference schemes is facilitated by use of a structured staggered Cartesian mesh. Complex stationary or rotating geometries are handled using an immersed boundary method (IBM).[9] The code is parallelized using OpenMP[16] and runs efficiently on 8–12 processors typical of many of today's desktop machines. More details on the numerical methods used and their implementation can be found in Delorme et al.[2]

Geometry

The geometry studied here is a simplified pathological medical device (see Fig. 1a). It consists of a small axi-symmetric nozzle with a convergent section, a constant section throat and a sudden expansion section. The maximum and minimum diameters are
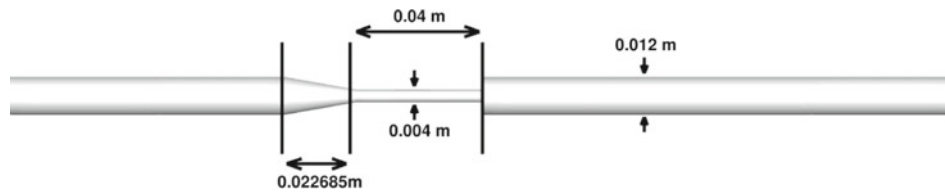
(a) Dimensions of the Idealized Medical device
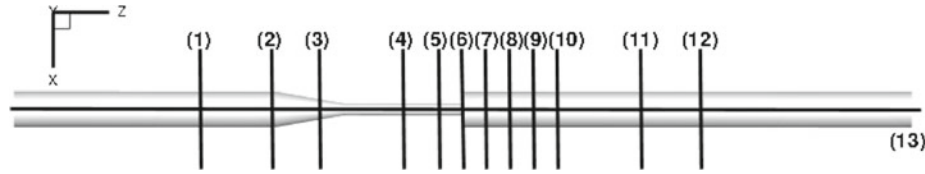
(b) Locations of the extracted data: Z = -0.088m (1), -0.064m (2), -0.048m (3), -0.020m (4), -0.008m (5), 0.000m (6), 0.008m (7), 0.016m (8), 0.024m (9), 0.032m (10), 0.060m (11), 0.080m (12), Centerline r=0 (13)

FIGURE 1. Geometrical characteristics of the FDA's idealized medical device.

0.012 and 0.004 m respectively. The geometry combines an accelerating section with increase in shear stresses, a high speed section, and a section with potential re-circulation zones. This idealized medical device shares most of the characteristics encountered in medical devices, such as tubing, catheters, or cannulae.

Figure 1b shows the locations where the data are extracted to make direct quantitative comparisons between numerical predictions and experimental measurements. The data are extracted along the centerline $r = 0$ (13), as well as at various locations along the nozzle. Sections (1) and (2) are located in the constant diameter inlet section. Section (3) is located inside the convergent section, while sections (4) and (5) are located further downstream in the high speed throat region. Section (6) ($Z = 0.000$ m) corresponds to the location of the sudden expansion. Sections (7)–(12) are located downstream of the expansion. These 13 sections are used to compare the velocity profiles, as well as the shear stresses with the experimental measurements. The wall pressures and shear stresses are extracted along the wall of the device and are averaged in the circumferential direction. At the sudden expansion location, data are averaged along the line $Z = 0.000$ m to account for possible variations of pressure and shear stresses along the wall at this location.

Flow Conditions and Simulation Details

The fluid is assumed Newtonian with a density $\rho = 1056$ kg/m³ and a dynamic viscosity of $\mu = 3.5 \times 10^{-3}$ N/s/m². Four different flow conditions are studied (see Table 1). At Re_t 500, the flow is laminar, even in the

post expansion region. At $Re = 2000$, the flow is transitional, while at $Re = 3500$ and $Re = 5000$, the flow is fully turbulent.[6] By considering these four cases, the LES code can be tested over the full range from laminar to turbulent flow.

The domain is $0.015 \times 0.015 \times 0.3$ m³. In LES, grid independence is related to sufficient resolution of the large-scale(filtered) flow field for a given filter width. A grid independence study was performed for the transitional case ($Re_t = 2000$): three different computational meshes were used to compute the flow field ($48 \times 48 \times 384$, $64 \times 64 \times 512$, and $96 \times 96 \times 768$). The difference in mean velocities between the two first grids were about 15% in average. The difference between the two last grids were less than 5% in average, and in agreement with the available experimental data from Hariharan *et al.*[6] All the simulations were run on this uniform Cartesian $64 \times 64 \times 512$ mesh resulting in approximately 2 million grid points. The time step is chosen to keep a Courant–Friedrichs–Lewy (CFL) number lower than 0.1 to ensure stability. At the inlets, a laminar velocity profile is imposed, as shown in Eq. (5).

$$\bar{u} = 2\bar{u}_{\text{mean}} \left(1 - \frac{r^2}{(D_{\text{inlet}}/2)^2}\right) \qquad (5)$$

where $\bar{u}_{\text{mean}}$ is the mean velocity as shown in Table 1, r is the radial location at the inlet face ($r = \sqrt{x^2 + y^2}$) and D_{inlet} is the diameter of the inlet ($D_{\text{inlet}} = 0.012$ m). At the outlet, a homogeneous Neumann boundary condition is imposed for all velocity components, assuming a fully developed flow, and a constant value Dirichlet boundary condition is imposed for the pressure. Each

simulation is run for 15 flow through time in order to obtain converged statistics for comparisons with experimental measurements. For the laminar and transitional cases, the simulations were performed using eight processors for a total of wall clock time of two weeks. For the turbulent cases, simulations were run using the same number of processors for a total wall clock time of 3–4 weeks.

RESULTS

Instantaneous Flow Structures

In contrast to RANS simulations, which only predict mean flow statistics, LES simulates a wide range of unsteady three-dimensional large-scale flow structures. Because modeling is limited to the relatively small SGS, which are thought to be more universal regarding different geometries and flow conditions, there is a greater potential for increased accuracy. Also, the ability to predict instantaneous flow patterns including re-circulation zones should result in more accurate predictions of regions of flow stasis or high shear, which is important for thrombosis or hemolysis prediction. In the geometry being studied here, the ability to accurately capture the complex irregular vortical flow structures associated with the transition to turbulence in the sudden expansion section ($Z > 0.000$ m) is key. This can be observed in Fig. 2, which shows instantaneous flow structures for the laminar, transitional, and turbulent cases.

Figure 2a shows the instantaneous axial velocity field in the expansion region. The laminar nature of the flow is observed as the laminar jet does not break down. Figures 2b and 2c show iso-surfaces of the λ_2 criterion[7] colored by vorticity magnitude. When the flow becomes transitional (Fig. 2b), the jet flow breaks down at a delayed transition location (around Z/D_{inlet} = 4). When the flow is turbulent (Fig. 2c), the breaking down location happens much sooner (Z/D_{inlet} = 2). All these instantaneous observations are consistent with the flow features reported in Hariharan et al.[6] Being able to accurately predict the transition from laminar to turbulent is critical when evaluating a medical device, especially since most pathological flows are transitional by nature.

Centerline Velocity Distribution

In the previous section we showed that the different flow regimes significantly impact the behavior of the flow in the post-expansion region. Similar comments can be made when looking at Fig. 3 which shows the centerline axial mean velocity distribution along the nozzle for all Re_t, with comparisons with experimental measurements.[6] For the laminar case (Fig. 3a), it can be seen that the velocity slowly decreases as the flow travels downstream indicating no breaking down of the jet. Agreement with experiments is within 95% of the confidence interval. For the transitional case (Fig. 3b), the

TABLE 1. Flow conditions studied in the present paper.

Case	Inlet Re	Throat Re_t	Inlet mean axial velocity (m/s)
1	167	500	0.0461
2	667	2000	0.1839
3	1167	3500	0.3218
4	1667	5000	0.4606

(a) $Re_t = 500$: Instantaneous axial velocity field

(b) $Re_t = 2000$: Instantaneous coherent structures, identified by the λ_2 criterion ($\lambda_2 = -10$), colored by vorticity magnitude

(c) $Re_t = 3500$: Instantaneous coherent structures, identified by the λ_2 criterion ($\lambda_2 = -10$), colored by vorticity magnitude
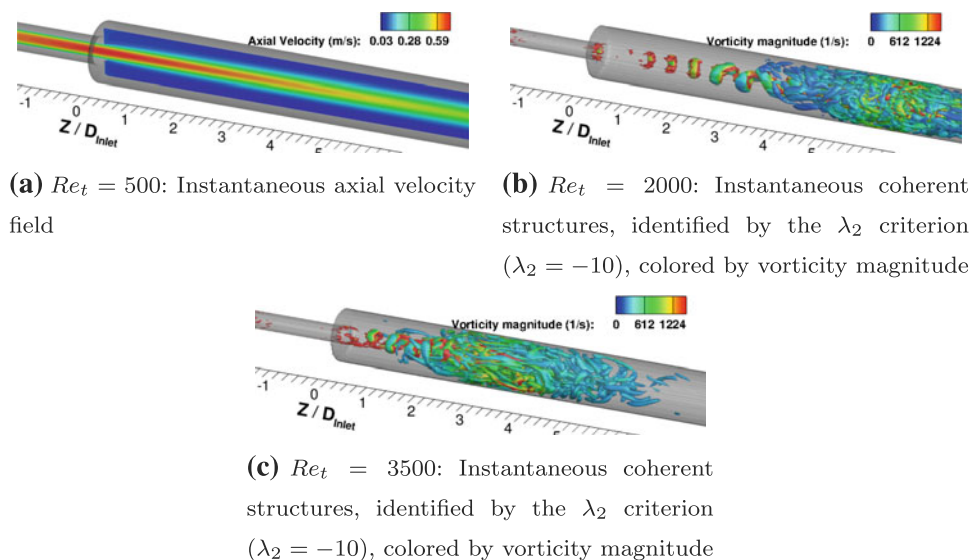
FIGURE 2. Instantaneous flow features for the laminar ($Re_t = 500$), transitional ($Re_t = 2000$), and turbulent ($Re_t = 3500$) cases.
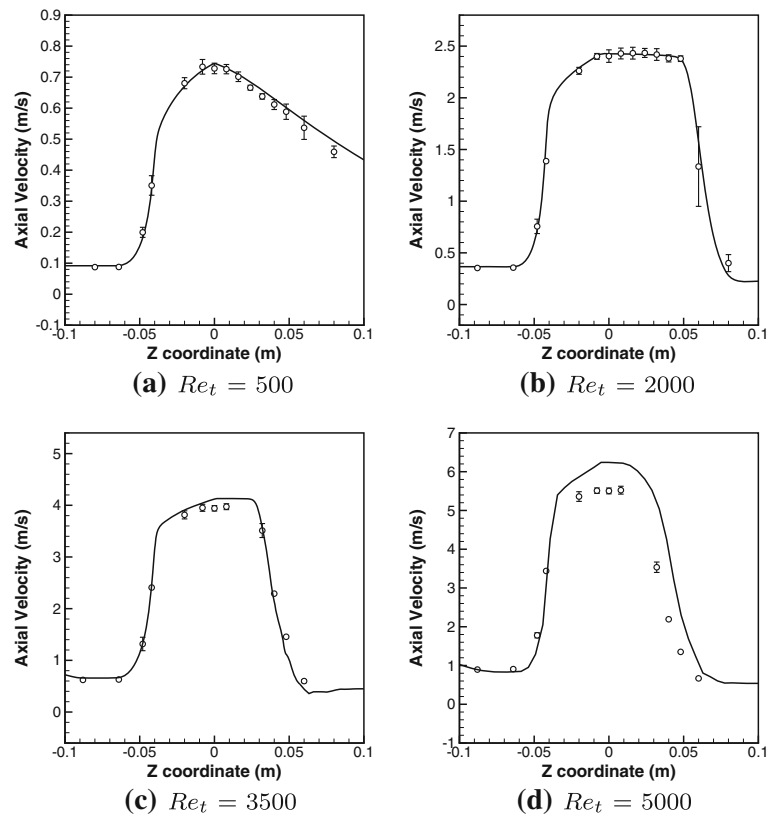
FIGURE 3. Nozzle mean centerline velocity (line: LES, symbols: experimental means ± 95% confidence interval from Hariharan *et al.*[6]).

velocity profile abruptly changes around $Z = 0.05$ m which is consistent with the delayed transition of the jet. Here, again, the prediction of the location of the breaking down of the jet is within 95% of the experimental confidence interval. For the two turbulent cases (Figs. 3c and 3d), the breaking down of the jet occurs much sooner (around $Z = 0.03$ m and $Z = 0.02$ m for $Re = 3500$ and 5000 respectively). At Re_t of 3500, the agreement with experiments is again within 95% of the experimental confidence of interval. By imposing a laminar parabolic velocity profile at the inlet, the laminar profile before the convergent section is well captured. At Re_t of 5000, the simulations predicted accurately the centerline velocity in the inlet and convergent sections. But in the throat and sudden expansion regions, the LES simulations over-predicted the centerline peak value of the mean axial velocity (between 20 and 45%). Also, the location of the breaking down of the jet downstream of the sudden expansion is under-predicted (about 0.01 m further away than in the experiments). These discrepancies are due to an under-estimation of the turbulent nature of the flow: the LES simulation predicts velocity profiles more parabolic (less turbulent) than experiments, which results in an over-estimation of the peak centerline velocity.

Wall Pressure Distribution

Because pressure fluctuations are known to activate platelets, characterization of a pathological medical device usually involves the study of the pressure field in the domain. Pressure is also commonly used to study the power loss inside medical devices, as well as characterize the performance of pumps.[8] Figure 4 shows the wall pressure distribution along the nozzle. We can see that for all cases, as the flow accelerates in the convergent section, the pressure decreases. In the sudden expansion region, the pressure stabilizes to a more constant value. All the results are plotted relative to the pressure at $Z = 0.000$ m. At $Re_t = 500$, the pressure drop in the convergent section is well predicted, but the pressure in the constant inlet area and sudden expansion is under-predicted (by 20%). At $Re_t = 2000$ and 3500, the predicted data are within 95% of the experimental confidence interval. At $Re_t = 5000$, the LES over-predicts the pressure in the inlet section (by 20%). The pressure drop in the convergent section is better predicted. Downstream of the sudden expansion, the numerical predictions are for most of the data within 95% of the experimental confidence interval, even though a slight under-shoot

can be seen when the turbulent jet breaks down. This may be due to a lack of grid resolution and is further detailed in the "Discussion" section.

Radial Distribution of Axial Velocity Profiles

Figures 5–8 show mean axial velocity profiles along several radial locations (locations $Z = -0.048$ m, $Z = 0.024$ m, and $Z = 0.060$ m are not shown here due to limitations on the number of figures) for Re_t of 500, 2000, 3500, and 5000, respectively. For the laminar case, Fig. 5 shows that the numerical predictions are all within the confidence interval of the experiments. The laminar velocity profiles in the inlet section are well captured (Figs. 5a and 5b). In the convergent and throat regions, the acceleration of the flow is well captured, with a fully developed profile just before the sudden expansion (Figs. 5c and 5d). Downstream of the sudden expansion, the velocity profiles become wider and wider, consistent with the slow spreading of the laminar jet. The slight reverse flow close to the walls is also in agreement with the experimental measurements (Figs. 5f–5i).

Similar comments can be made for the transitional case (Fig. 6). The numerical predictions are within the 95% confidence interval except for the convergent and throat section. In the inlet region, a laminar parabolic velocity profile is seen, in agreement with the experimental measurement (Figs. 6a and 6b). In the convergent and throat sections, the velocities show a flatter profile (for $0 < r < 0.001$ m) consistent with the more turbulent nature of the flow. The flow in the experiments seems to develop faster than in the simulations (Figs. 6c and 6d). Numerical predictions are within the interval of confidence of the experiments at the end of the throat section (Fig. 6e). Downstream of the sudden expansion, the simulations predicted very well the blunted jet with delayed break down (Figs. 6f–6h). At $Z = 0.080$ m, the jet breaks down as shown by the drop of centerline velocity, in agreement with experimental measurements (Fig. 6i).

Figure 7 shows the comparisons between LES and experiments for the case at $Re = 3500$. Even though the flow is turbulent, the inlet conditions in the experiments are laminar. By keeping the inlet section short in the LES simulations, parabolic velocity profiles within 95% confidence interval of the experiments are observed (Figs. 7a and 7b). Similarly to the transitional case, in the convergent and throat sections, the LES solver does not predict a flow that develops as fast
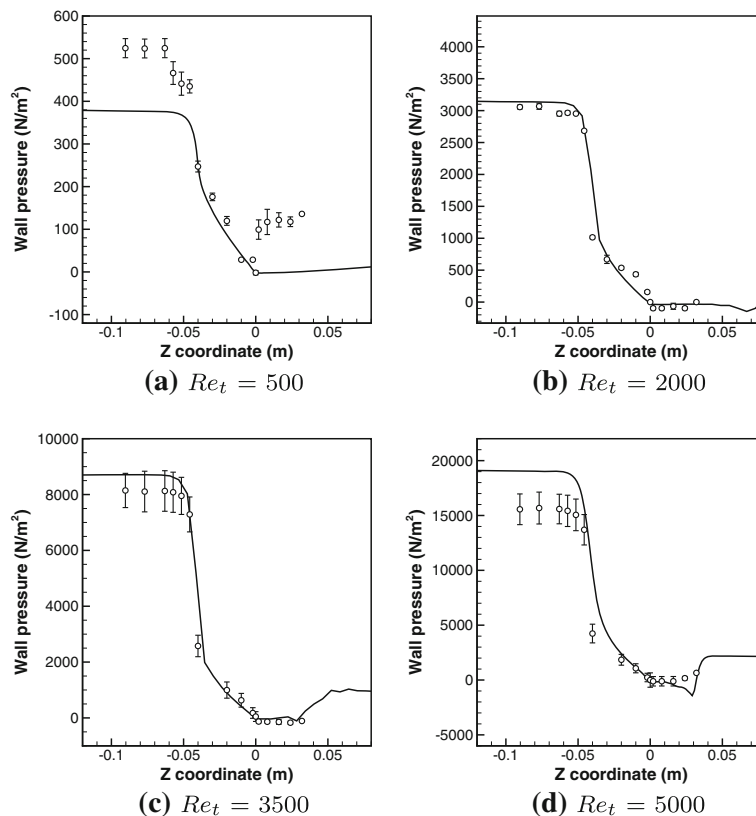

(a) $Re_t = 500$

(b) $Re_t = 2000$

(c) $Re_t = 3500$

(d) $Re_t = 5000$

FIGURE 4. Nozzle mean wall pressure (line: LES, symbols: experimental means ± 95% confidence interval from Hariharan et al.[6]).

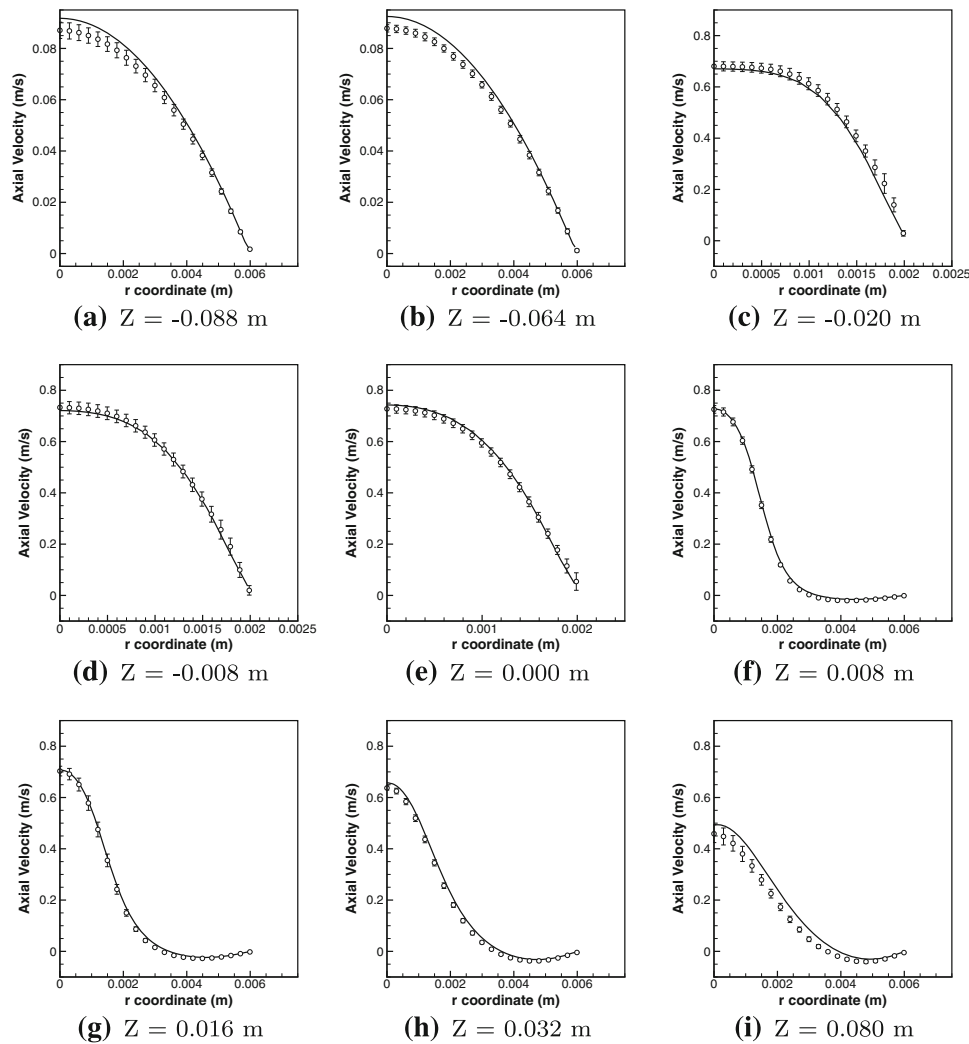**FIGURE 5.** Mean axial velocity profiles for Re_t = 500 (line: LES, symbols: experimental means ± 95% confidence interval from Hariharan *et al.*[6]).

as in the experiments (Figs. 7c and 7d). Indeed, we can see that the LES predicts accurately the peak of the velocity, as well as the flat profile typical of a turbulent flow, but the velocity decreases earlier in the simulation compared to the experiments. By the end of the throat section, LES predictions are again within the 95% confidence interval of the experimental measurements (Fig. 7e). Early downstream of the sudden expansion, numerical simulations predict the shape of the developing jet, with the rapid change of velocity as we move closer to the walls (Figs. 7f and 7g). At $Z = 0.032$ m, the jet starts breaking down. The LES predicts a more abrupt change of velocity compared to the experiments, with less re-circulating flow (Fig. 7h). This slight delay can also be observed on Fig. 7i, where experiments show a fully developed turbulent velocity profile, whereas the numerical predictions show a

slight overshoot of the velocity magnitude (about 15% above the measured value).

Figure 8 shows the comparisons between LES and experiments for the case at $Re = 5000$. Due to the laminar velocity profile imposed at the inlet, parabolic velocity profiles at $Z = -0.088$ m and $Z = -0.064$ m are observed and are in agreement with the experimental measurements (Figs. 12a and 12b). In the convergent and throat sections, the flow develops towards a turbulent flow faster in the experiments than in the numerical predictions, as seen in Figs. 8c–8e. This results in an overshoot of the peak velocity ($+0.5$ m/s) for the LES simulations. Early downstream of the expansion, LES predicts accurately the abrupt change of velocity, but the peak of the velocity is still overestimated by 20% (Figs. 8f and 8g). Figure 8h shows that, as already seen on Fig. 3d, the LES simulations
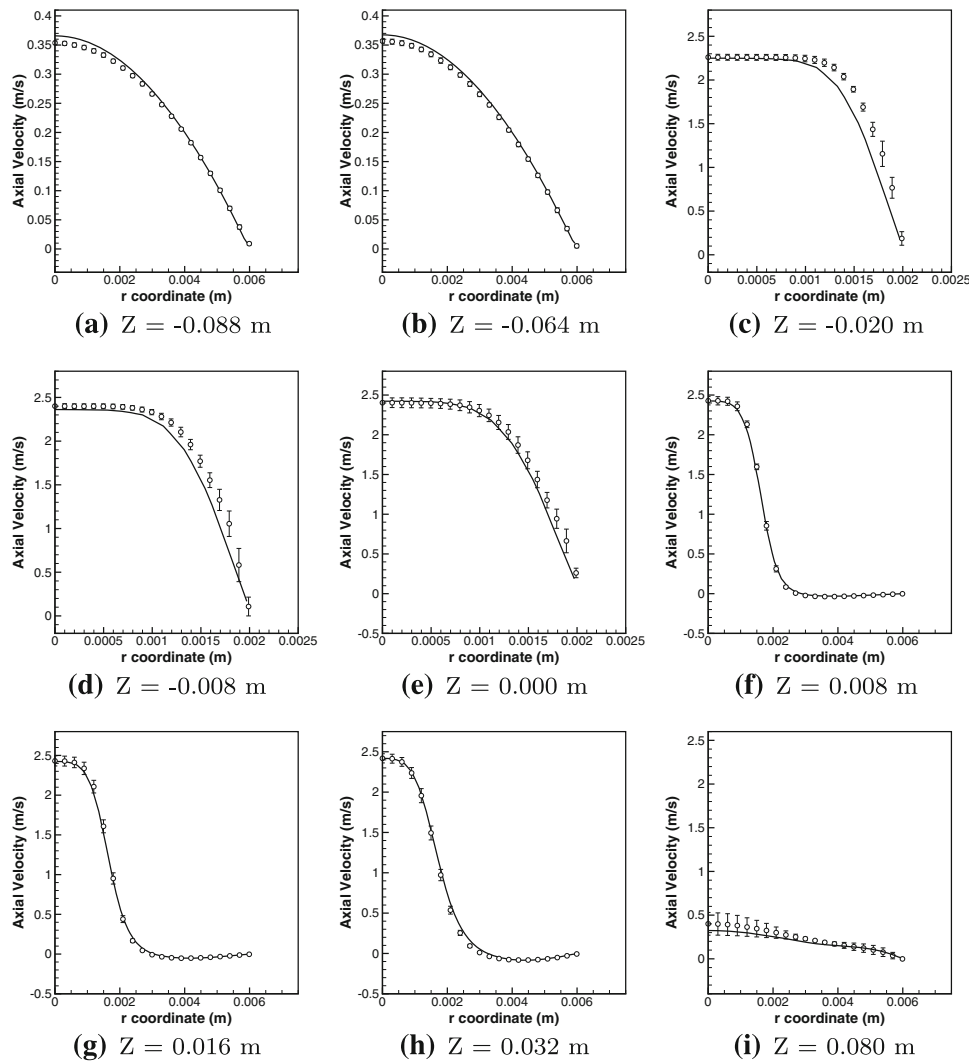
FIGURE 6. Mean axial velocity profiles for Re_t = 2000 (line: LES, symbols: experimental means ± 95% confidence interval from Hariharan *et al.*[6]).

over-estimate the location of the breaking down of the turbulent jet, resulting in a slower drop of the peak velocity compared to the experiments (around 60% of maximum error). But further downstream, the flow becomes fully turbulent in agreement with the experimental measurements (Fig. 8i).

Fluid Shear Stress Profiles

The magnitude of the shear stress is a very important measure when assessing pathological and medical device hemodynamics as it relates directly to hemolysis and platelets activation.[5,13] The shear stress magnitude is defined as:

$$|\tau| = 2\mu\sqrt{S_{ij}S_{ij}} \qquad (6)$$

where S_{ij} and μ are the components of the strain rate tensor and the dynamic viscosity, respectively, as

defined in "Methods" section. Figures 9–12 show mean shear stress magnitude profiles at several Z locations for Re_t 500, 2000, 3500, and 5000, respectively. Figure 9 shows the shear stress magnitude profiles for the laminar case. In the inlet section, we can see that both LES and experiments show a linear profile consistent with a laminar flow. But the magnitude of the LES predictions is in average twice larger than the experimental observations (Figs. 9a and 9b). This is due to the fact that the velocity profiles have slightly more turbulent nature compared to the experiments. In the convergent and throat sections, the LES predictions over-predict the increase of shear stresses as we move close to the wall (Figs. 9c–9f). The peak value of the stresses are comparable between simulations and measurements in the convergent and early in the throat (Figs. 9c and 9d), but LES over-predicts the rise and the peak of the stresses at the
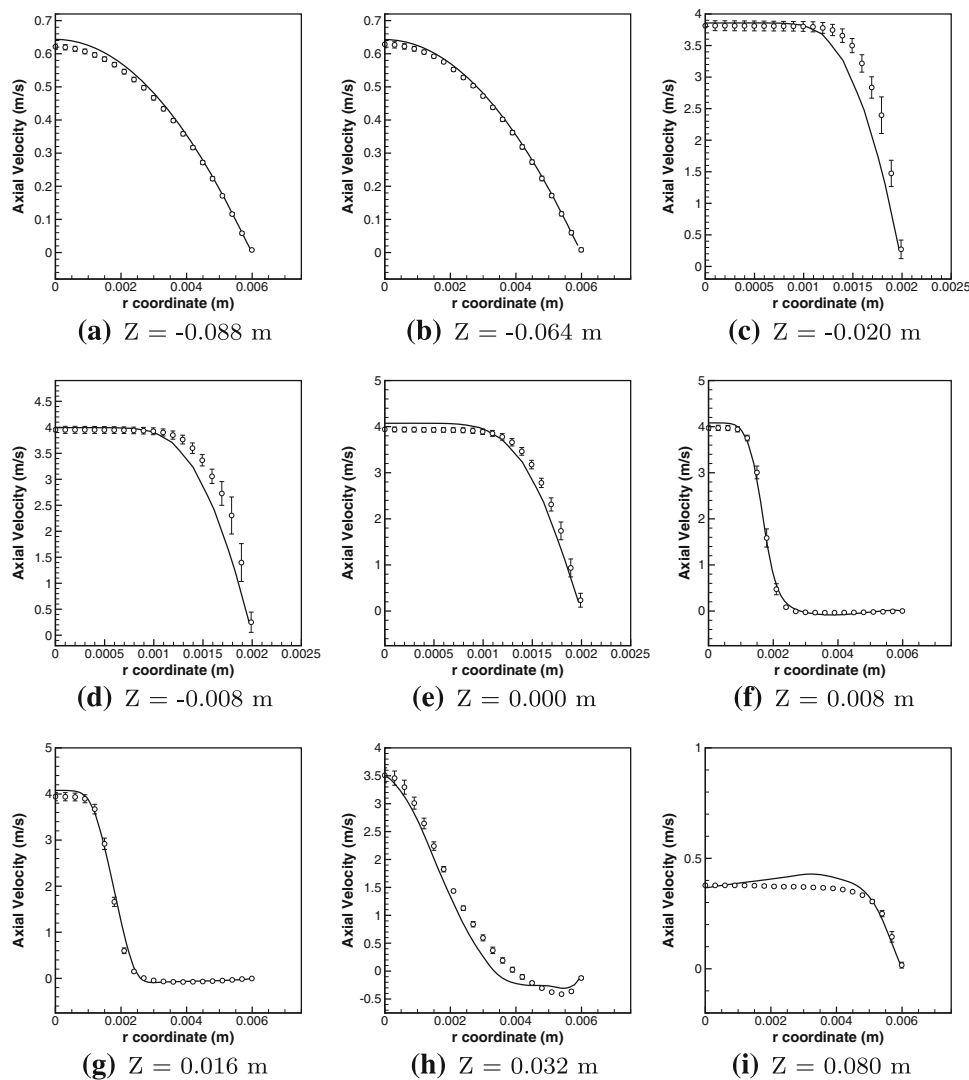
FIGURE 7. Mean axial velocity profiles for Re_t = 3500 (line: LES, symbols: experimental means ± 95% confidence interval from Hariharan *et al.*[6]).

expansion location by 80% (Fig. 9e). Downstream of the sudden expansion, LES over-predicts the peak of stresses compared to the experiments by about 40% (Figs. 9f–9i). However a qualitative agreement can be observed: LES simulations capture the main peak due to the drop of velocity, as well as the secondary peak closer to the wall where re-circulation happens.

For the transitional case (Fig. 10), very similar comments can be made. In the inlet section, LES predicts a linear profile consistent with the laminar nature of the flow, but the magnitude is about twice larger compared to the experiments (Figs. 10a and 10b). In the convergent and throat sections, the accelerating fluid results in an increase in stresses: LES slightly over-predicts the rate at which the shear stresses increase as we move closer to the wall, and slightly under-predicts the peak magnitude of the

stresses (between 15 and 20%) (Figs. 10c and 10d). At the expansion location, LES over-predicts the peak of shear stresses by about 35% (Fig. 10e). Downstream of the expansion, we have a qualitative agreement between LES predictions and experiments, but LES over-estimates the peak of shear stresses by about 40% (Figs. 10f–10h). Further downstream, slight disagreement (shear stresses higher in the simulation by 40% in average compared to the experiments) can be seen between LES and experiments, consistent with the difference of velocity shown before (Fig. 10i).

At Re_t of 3500, the shear stress magnitude increases everywhere inside the nozzle compared to the laminar and transitional flows. Linear profiles with twice larger values of the shear stresses are seen in the inlet region (Figs. 11a and 11b). LES over-estimates the rate at
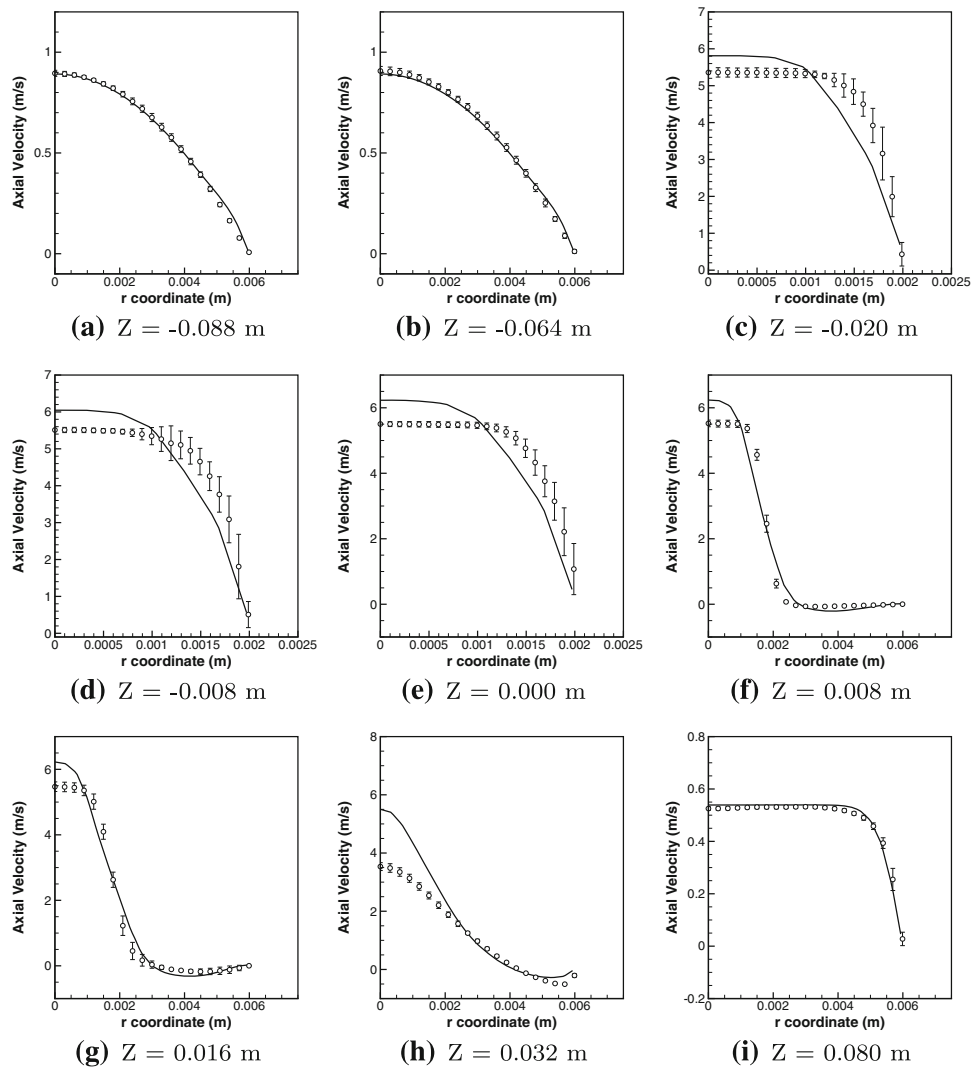
FIGURE 8. Mean axial velocity profiles for Re_t = 5000 (line: LES, symbols: experimental means ± 95% confidence interval from Hariharan *et al.*[6]).

which the shear stresses increases in the radial direction in the convergent and throat regions (Figs. 11c–11e). In the convergent section, the peak value is similar between the numerical simulations and experiments. At the sudden expansion, LES over-predicts the predicted value by 30%. Early downstream of the expansion, LES slightly over-predicts the value of the peak of the shear stresses (by about 20%), but qualitative agreement is observed (Figs. 11f and 11g). Figure 11h shows that, further downstream of the expansion, LES over-predicts by 60% the magnitude of the first peak, but accurately capture the magnitude and location of the secondary peak close to the wall. Further downstream, the flow is fully turbulent and the numerical predictions are within the 95% confidence interval of the experimental measurements (Fig. 11i).

At Re_t of 5000 (Fig. 12), the agreement in the laminar regions (Figs. 12a and 12b) is better than for the other Reynolds numbers presented: LES does not over-predict as much the peak magnitude compared to the other Reynolds numbers (about 50% error). In the throat section (Figs. 12c–12e), LES slightly under-predicts the magnitude of shear stresses close to the walls (40–50%), but still over-predicts the rate at which the shear stresses increase. Figures 12f and 12g show that the numerical predictions agree with the experimental data. At Z = 0.032 m, the agreement is not as good since the LES did not predict a fully turbulent flow profile as early as in the experimental measurements. The shear stresses are under-estimated by about 30%. But at Z = 0.080 m (Fig. 12i), numerical predictions are within the confidence interval of the
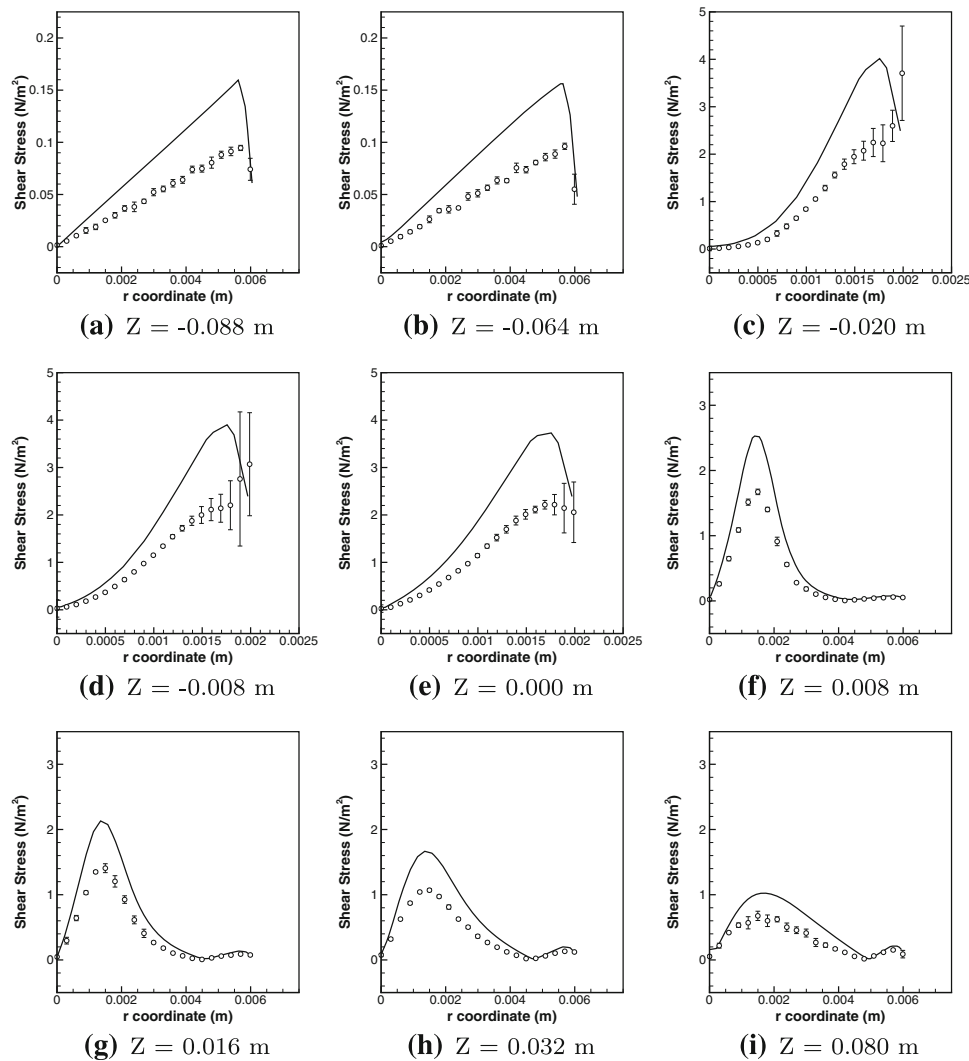
FIGURE 9. Mean shear stress magnitude profiles for $Re_t = 500$ (line: LES, symbols: experimental means ± 95% confidence interval from Hariharan *et al.*[6]).

experimental measurements, with a profile typical of a fully turbulent flow.

Wall Shear Stress Distribution

Another important hemodynamic measure to extract from CFD results is wall shear stresses. Pathological flows usually induce high wall shear stresses and better prediction tools could help with evaluation of performance and bio-compatibility of a medical device.[5] In their paper, Stewart *et al.*[12] show that a wide range of behavior was observed for all the turbulence models when trying to predict the wall shear stresses. Most models are able to predicts the wall shear stresses in the throat region. Most models overestimate the value of the wall shear stresses in the inlet section, and discrepancies are observed early downstream of the sudden expansion. Most models show a

peak in stresses at each sudden change of geometry (convergent/throat and throat/expansion). Figure 13 shows the comparisons between the wall shear stresses from LES predictions and the experimentally measured wall shear stresses for all Reynolds numbers. The wall shear stresses are computed following the approach of Mark *et al.*[9] The values of the wall shear stresses are averaged in the circumferential direction.

All profiles are within the 95% confidence interval of the experimental measurements (Figs. 13a–13d). A wide range of values is observed for the experimental measurements, due to the difficulty to measure velocities very close to the wall. But overall, the LES predictions are in agreement with the mean experimental measurements. The numerical simulations predict the fast increase of wall shear stresses in the convergent section due to the acceleration of the fluid. In the throat section, the wall shear stresses increase but at a
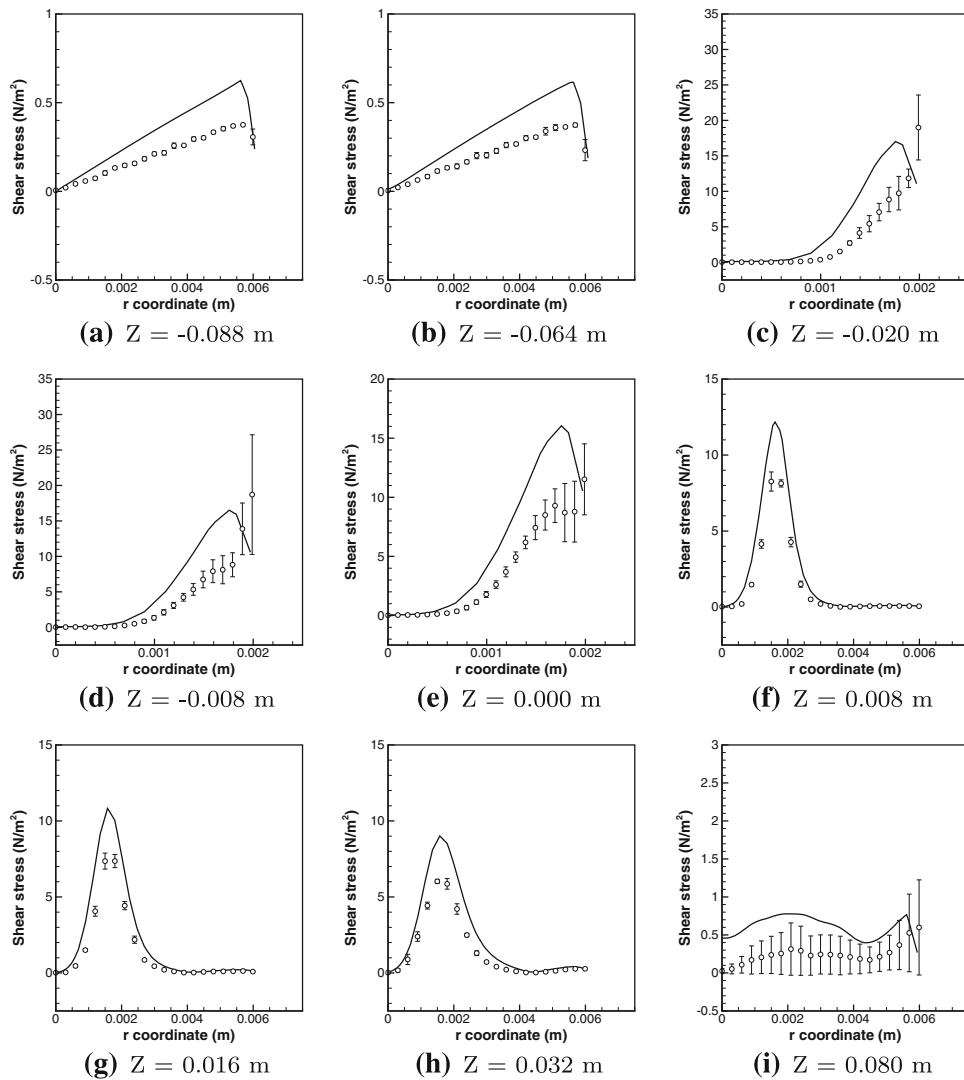
FIGURE 10. Mean Shear stress magnitude profiles for Re_t = 2000 (line: LES, symbols: experimental means ± 95% confidence interval from Hariharan *et al.*[6]).

slower rate. At $Z = 0.000$ m, the wall shear stresses drop rapidly corresponding to the re-circulation zone and are accurately predicted by the simulations. The wall shear stresses in the inlet region are slightly over-predicted (up to 5 N/m^2 higher for $Re_t = 5000$). The simulations do not over-predict the values of the stresses when the geometry changes suddenly, making it useful for blood damage estimation in general.

DISCUSSION

Summary of the Results

In their recent paper, Stewart *et al.*[12] emphasize the experimental and computational challenges associated with this geometrically simple idealized medical device with no moving parts. Even at low Reynolds number,

the flow field shows laminar, transitional, and turbulent flow features that are often difficult to predict for some of the typical RANS turbulence models.[14] A turbulence model usually assumes a particular flow regime, and accurate predictions are sometimes difficult to obtain if all flow regimes are present in the computational domain at once. Inaccuracies in mean velocity predictions would then result in poor predictions of fluid and wall shear stresses since these depend on derivatives of the velocity field. In order to improve accuracy of the results, as well as the predictions of performance of a device, a careful study of the physics of the flow of interest is necessary to choose the suitable turbulence model.

The present study represents one of the first attempts at LES for this idealized medical device benchmark case. The in-house code (*WenoHemo*™)
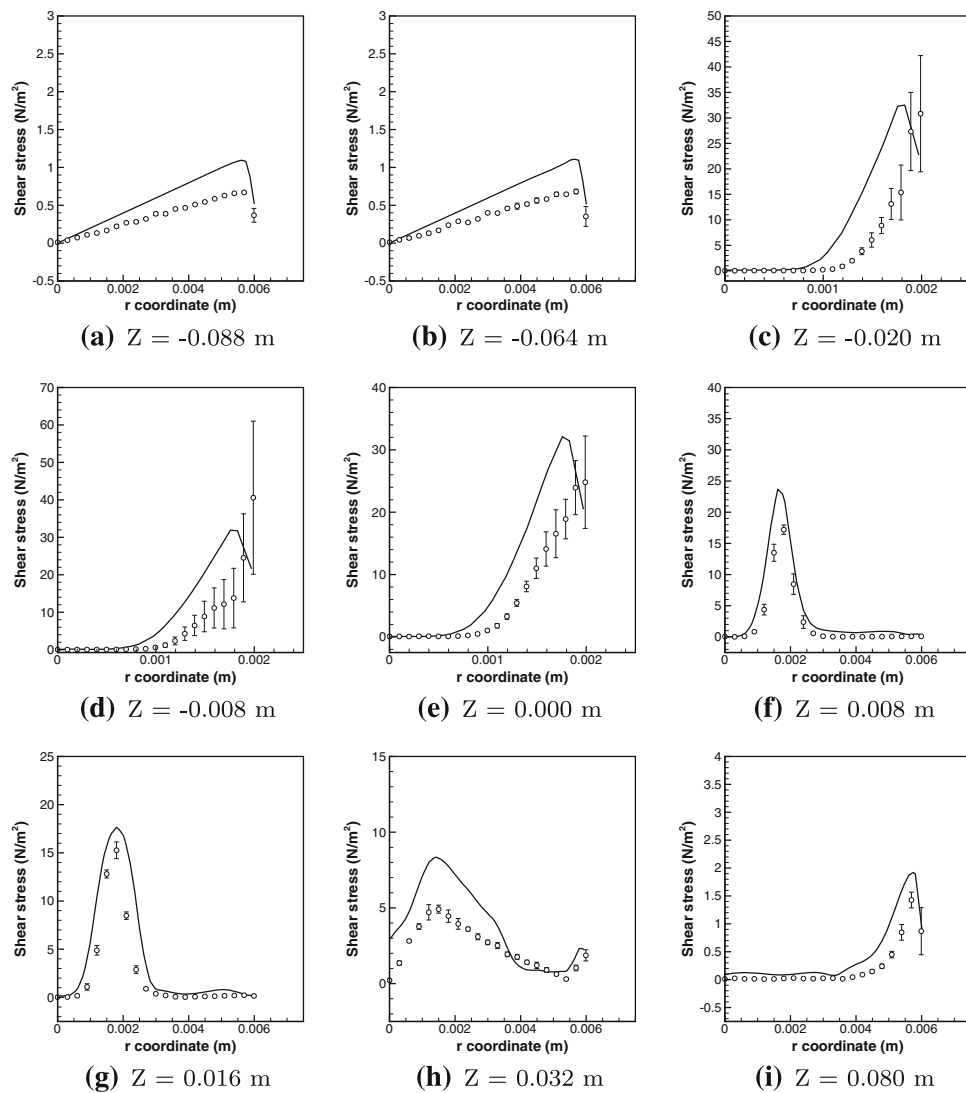
FIGURE 11. Mean shear stress magnitude profiles for Re_t = 3500 (line: LES, symbols: experimental means ± 95% confidence interval from Hariharan *et al.*[6]).

numerically integrates the filtered incompressible Navier–Stokes equations by combining high-order finite-difference methods with an IBM to handle complex geometries on a simple to generate structured Cartesian meshes.

At Re_t 500, LES successfully captures the laminar nature of the flow, as observed in the experiments.[6] The jet developing in the sudden expansion region is laminar and does not break down, as shown by the centerline axial velocity distribution along the nozzle. The numerical simulations accurately predict the drop of pressure and shear stresses downstream of the sudden expansion. However they are not able to capture the magnitude of the wall pressure in the inlet section, similarly to the results shown by Stewart *et al.*[12] The agreement between the LES and experiments for the fluid shear stresses is only qualitative, with a good

prediction of the two peak locations for the stresses where the gradient of velocity is the highest.

At Re_t 2000, the experiments show a transitional flow with a delayed breaking down of the jet downstream of the expansion. In the simulations, the location of the breaking down is accurately predicted and is visible on the pressure and wall shear stress profiles. In the contraction and throat sections, the velocity profiles show a slightly more turbulent nature of the flow for the experiments compared to the numerical simulations. Similarly to the laminar case, LES overpredicts the peak values of the fluid shear stresses.

At Re_t 3500 and 5000, the flow becomes turbulent, showing an earlier break down of the jet after $Z = 0.000$ m. For the most turbulent case, LES is not able to accurately predict the location of the jet break down (over estimating the downstream location by
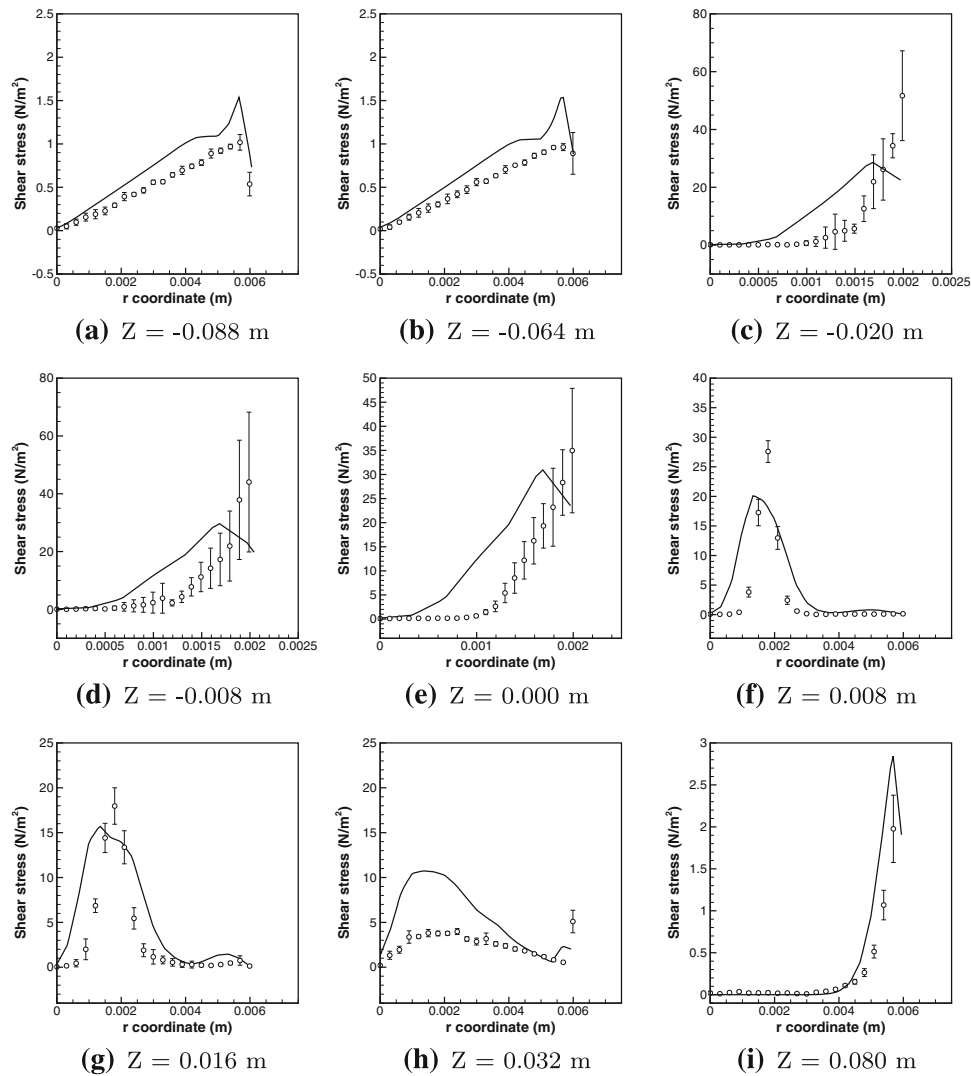
FIGURE 12. Mean shear stress magnitude profiles for Re_t = 5000 (line: LES, symbols: experimental means ± 95% confidence interval from Hariharan *et al.*[6]).

about 0.01 m). At Re_t = 3500, the numerical predictions for the velocity are close to the confidence interval of the experimental measurements. The experiments showed a slightly more turbulent nature of the flow. Similarly, at Re_t = 5000, the experimental flow field is more turbulent, which results in an over-prediction of the peak velocity in the LES simulations. In the convergent and throat sections, the agreement for the fluid shear stresses is mostly qualitative, with an under-estimation of the peak value. Downstream of the sudden expansion, LES predictions are mostly over-predicting the value of the stresses. The disagreement between numerical predictions and experiments are thought to be related to a possible lack of grid resolution at these higher Re_t. Indeed, grid independence is achieved for the transitional case, but has not been shown for the more turbulent cases.

Validation Parameter

Figure 14 shows a summary of the performance of the solver for all Reynolds number. It shows a validation metric parameter[12] along the nozzle. This parameter is defined as:

$$E = \frac{1}{N} \sum_{i=1}^{N} \left| \frac{\bar{u}_{\text{exp},i} - \bar{u}_{\text{cfd},i}}{\bar{u}_{\text{exp},i}} \right| \qquad (7)$$

where E is the validation parameter, $\bar{u}_{\text{exp},i}$ are the mean experimental axial velocities at a constant Z location, $\bar{u}_{\text{cfd},i}$ are the mean LES axial velocities at a constant Z location and N is the number of data points taken into account along the radial direction. For each case, 41 data points are considered to compute E, but only values above 0.01 m/s are kept to avoid artificial increase of the parameter due to very small values of
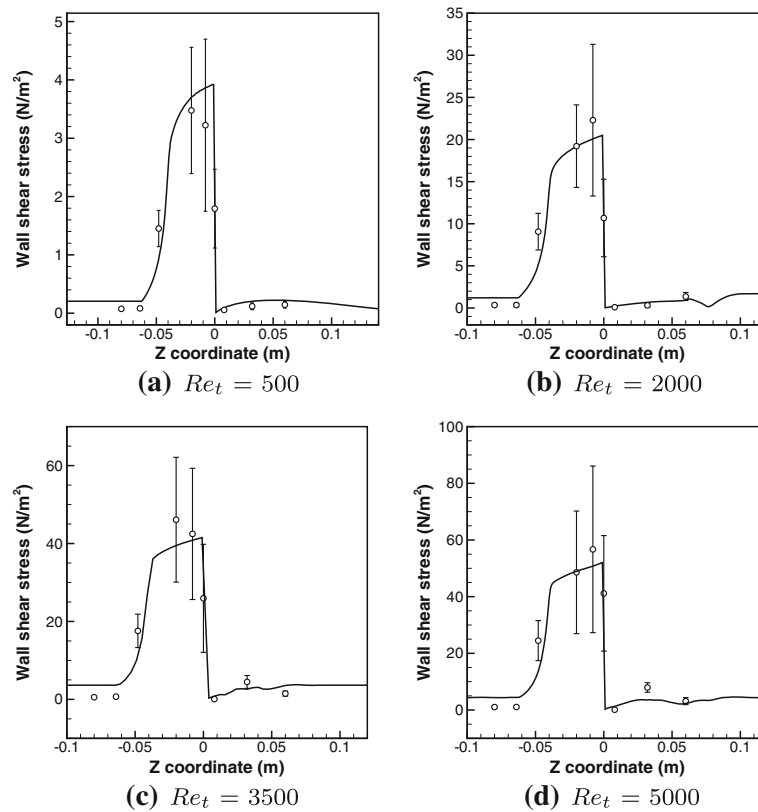
FIGURE 13. Nozzle mean wall shear stress (line: LES, symbols: experimental means ± 95% confidence interval from Hariharan et al.[6]).
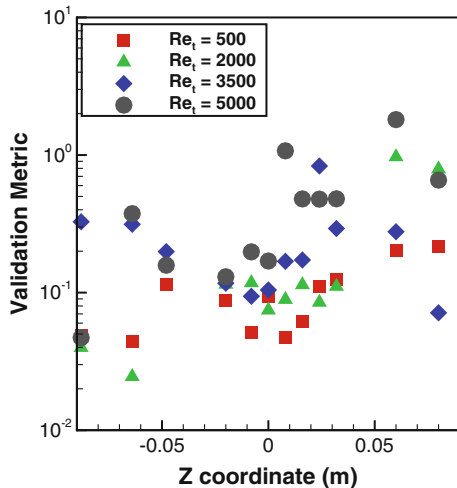

FIGURE 14. Local validation metric for all Reynolds numbers.

the velocity. This parameter allows us to compute how close are the LES predictions to the experimental measurements (the closer the value to 0, the more accurate the LES results).

In the constant diameter inlet region, the error is close to $E = 0.1$ at all Reynolds number due to the laminar profile imposed at the inlet boundary. In the convergent and throat regions, the results also show an error very close to $E = 0.1$ or below. Downstream of the sudden expansion, different behavior can be seen. For the laminar case, the error stays low (close to $E = 0.1$) all the way to the outlet. At $Re_t = 2000$, the error stays low early downstream of the expansion ($E = 0.1$) but increases when the jet breaks down (E close to 1). This error is mostly due to differences in low values of the velocities close to the wall. At $Re_t = 3500$, the error increases around $Z = 0.032$ m ($E = 1$) but decreases again as we move further downstream (E lower than 0.1 at $Z = 0.080$ m). At $Re_t = 5000$, the error is larger due to the under-prediction of the turbulent nature of the flow. The error still stays lower than 2 at maximum.

CONCLUSION

Predicting transitional flows, those that involve both laminar and turbulent regions, is challenging for any CFD model. The main advantage of LES over RANS in this regard is that with LES transition can be captured more naturally, without having to change the turbulence model as the regime of the flow changes. In

this study, the application of LES to relatively complex geometries and transitional flows is made possible by combining high-order numerical methods on structured Cartesian grids with IBM and a transition sensitive SGS model (see Delorme *et al.*[2]). Predictions of flow statistics in the FDA's idealized medical device are shown to be in agreement with the experimental results from Hariharan *et al.*[6] for the mean velocities at $Re_t = 500$, 2000, and 3500. Discrepancies at $Re_t = 5000$ can be seen, as well as a consistent over-prediction of the fluid shear stresses inside the device for all Re_t. In the inlet and convergent sections, as the flow accelerates, this study shows that LES is capable of capturing the laminar and transitional nature of the flow. But after the sudden expansion, as a jet forms and breaks down, the study shows that largest differences between predictions and measurements can be observed. These differences are thought to be due to a lack of grid resolution and could result in over-predictions of blood damage. Studies about the effect of a grid refinement on the accuracy of the results at high Reynolds number will be performed in the future.

ACKNOWLEDGMENTS

REFERENCES

[1]Adams, J. http://www2.cisl.ucar.edu/resources/legacy/mudpack, 1999.
[2]Delorme, Y., K. Anupindi, A. Kerlo, D. Shetty, M. Rodefeld, J. Chen, and S. Frankel. Large eddy simulation of powered fontan hemodynamics. *J. Biomech.* 46:207–436, 2013.
[3]Durbin, P., and B. P. Reif. Statistical Theory and Modeling for Turbulent Flows. Hoboken: Wiley, 2010.
[4]Fraser, K., E. Taskin, B. Griffith, and Z. Wu. The use of computational fluid dynamics in the development of ventricular assist devices. *Med. Eng. Phys.* 33:263–280, 2011.
[5]Fraser, K., T. Zhang, B. Griffith, and Z. Wu. A quantitative comparison of mechanical blood damage parameters in rotary ventricular assist devices: shear stress, exposure time and hemolysis index. *J. Biomech. Eng.* 134:081002, 2012.
[6]Hariharan, P., M. Giarra, V. Reddy, S. Day, K. Manning, S. Deutsch, S. Stewart, M. Myers, M. Berman, G. Burgreen, and E. Paterson. Multilaboratory particle image velocimetry analysis of the FDA benchmark nozzle model to support validation of computational fluid dynamics simulations. *J. Biomech. Eng.* 133:041002, 2011.
[7]Jeong, J., and F. Hussain. On the identification of a vortex. *J. Fluid Mech.* 285:69–94, 1995.
[8]Kennington, J., S. Frankel, J. Chen, S. Koenig, M. Sobieski, G. Giridharan, and M. Rodefeled. Design optimization and performance studies of an adult scale viscous impeller pump for powered fontan in an idealized total cavopulmonary connection. *Cardiovasc. Eng. Technol.* 2:237–243, 2011.
[9]Mark, A., and B. van Wachem. Derivation and validation of a novel implicit second order accurate immersed boundary method. *J. Comput. Phys.* 227:6660–6680, 2008.
[10]Shetty, D., T. Fisher, A. Chunekar, and S. Frankel. High order incompressible large eddy simulation of fully inhomogeneous turbulent flows. *J. Comput. Phys.* 229:8802–8822, 2010.
[11]Shetty, D., S. Jie, A. Chandy, and S. Frankel. A pressure correction scheme for rotational Navier–Stokes equations and its application to rotating turbulent flows. *Commun. Comput. Phys.* 9:740–755, 2011.
[12]Stewart, S., E. Patterson, G. Burgreen, P. Hariharan, M. Giarra, V. Reddy, S. Day, K. Manning, S. Deutsch, M. Berman, M. Myers, and R. Malinauskas. Assessment of cfd performance in simulations of an idealized medical device: results of FDA's first computational interlaboratory study. *Cardiovasc. Eng. Technol.* 3:139–160, 2012.
[13]Taskin, M., K. Fraser, T. Zhang, B. Gellman, A. Fleischli, K. Dasse, B. Griffith, and Z. Wu. Computational characterization of flow and hemolytic performance of the UltraMag blood pump for circulatory support. *Artif. Organs* 34:1099–1113, 2010.
[14]Varghese, S., and S. Frankel. Numerical modeling of pulsatile turbulent flow in stenotic vessels. *J. Biomech. Eng.* 125:445–460, 2003.
[15]Vreman, A. An eddy-viscosity subgrid-scale model for turbulent shear flow: algebraic theory and applications. *Phys. Fluids* 16:3670–3681, 2004.
[16]www.openmp.org/wp, 2012.
[17]Zhang, J., and T. Jackson. A high order incompressible flow solver with WENO. *J. Comput. Phys.* 228:2426–2442, 2009.